Applied Catalysis B: Environmental 132–133 (2013) 353–362

Contents lists available at SciVerse ScienceDirect

Applied Catalysis B: Environmental

journal homepage: www.elsevier.com/locate/apcatb

The improved reactivity of manganese catalysts by Ag in catalytic oxidation of toluene

Zhenping Qu[a,*], Yibin Bu[a], Yuan Qin[a], Yi Wang[a], Qiang Fu[b]

[a] Key Laboratory of Industrial Ecology and Environmental Engineering (MOE), School of Environmental Science and Technology, Dalian University of Technology, Linggong Road 2, Dalian 116024, China
[b] State Key Laboratory of Catalysis, Dalian Institute of Chemical Physics, Chinese Academy of Sciences, Dalian 116023, China

ARTICLE INFO

Article history:
Received 30 July 2012
Received in revised form 6 November 2012
Accepted 9 December 2012
Available online 20 December 2012

Keywords:
Toluene oxidation
Ag-Mn/SBA-15
Redox properties
Lattice oxygen
Interaction

ABSTRACT

The effects of Ag on Mn/SBA-15 catalysts have been investigated in the toluene catalytic oxidation. The reactivity of catalysts is related closely to the Ag/Mn molar ratio, and the sample with 1:3 of Ag/Mn molar ratio exhibits the highest reactivity for toluene oxidation, with a complete conversion at 260 °C. Based on the characterization results, it is found that Ag enters into MnO_2 phase, and the $Ag_{1.8}Mn_8O_{16}$ mixed phase forms. Meanwhile Ag leads to parts of MnO_2 being transformed into Mn_2O_3. The Ag/Mn molar ratio has a strong influence on the molar ratio of the surface Mn^{4+} to Mn^{3+} and surface adsorbed oxygen (O_{ads}) to lattice oxygen (O_{latt}) through the interaction between silver and MnO_x. The coexistence of MnO_2, Mn_2O_3, $Ag_{1.8}Mn_8O_{16}$, and the strong interactions between Ag and Mn species exhibit a good synergetic interaction, which promotes the reducibility of catalysts and the formation of abundant active lattice oxygen, thus increasing the catalytic activity of toluene oxidation. And the formation of intermediate benzaldehyde should be closely link with the lattice oxygen of the Mn based catalyst.

1. Introduction

Volatile Organic Compounds (VOCs) have always been hazardous to human health and environment, and toluene is one of typical gaseous pollutant among these VOCs. Although high efficiency of noble metals has been proved in the catalytic elimination of VOCs [1–3], attempts to make use of them are limited due to theirs high cost and low stability. In contrast, high stability and low cost make transition metal oxides (such Mn [4–7], Cu [8], Co [9,10]) much more available to some practical application. Therefore, it is of great scientific and practical interest to investigate the properties of transition metals oxides and improve their catalytic activity.

For transition metal oxides, it is well accepted that the oxidation of organic molecules involves a Mars and van Krevelen (MVK) mechanism, where the organic molecule is oxidized by lattice oxygen of metal oxides, the latter being re-oxidized by gas phase oxygen [10–14]. The lattice oxygen plays an important role in the catalytic oxidation of VOCs over transition metal oxides. It is well known that manganese oxides exhibit strong oxygen storage/release ability due to the fact that they easily undergo a rapid reduction–oxidation cycle through the interaction with reducing or oxidant agents, and accompany by the formation of manganese ions in various oxidation states [4,11]. Also manganese oxides have been proved to be highly active, durable and low cost, and they are applied as catalysts for the oxidation of volatile organic substances or hydrocarbons [4–6]. Manganese oxides, such as Mn_3O_4, Mn_2O_3 and MnO_2, are known to exhibit different activity in some catalytic oxidation reaction. Kim et al. reported that the reactivity shows an order of $MnO_2 < Mn_2O_3 < Mn_3O_4$ in the toluene oxidation [4]. Torres et al. reported that Mn^{4+} was more benefit for catalytic oxidation of formaldehyde [7]. MnO_2, Mn_2O_3 or the mixed oxides were identified as the active components in the CO oxidation and N_2O decomposition [15,16].

Much effort has been undertaken to improve the catalytic performance of manganese oxides. Santos et al. related the lattice oxygen of manganese oxides to the higher reactivity of manganese oxides towards oxidation of VOCs [11]. Wang et al. suggested that higher reactivity of OMS catalysts for the oxidation of ethanol and acetaldehyde can be assigned to the improvement of oxygen activation [12]. And many researchers have found that the lattice oxygen mobility of manganese oxides can be enhanced by doping other metal elements. The interaction between MnO_x and CeO_2 leads to the formation of more labile oxygen species in materials [17]. Morales et al. reported that the addition of Cu into Mn catalysts prevents manganese oxide reaching crystalline structure and enhances the existence of oxygen vacancies, which gives a best performance in ethanol combustion [18]. Gac et al. have found the decrease of Mn—O bonds strength due to the silver effect is useful for the

* Corresponding author. Fax: +86 411 84708083.
E-mail addresses: quzhenping@dlut.edu.cn, zhenpq@dicp.ac.cn (Z. Qu).

0926-3373/$ – see front matter © 2012 Elsevier B.V. All rights reserved.
http://dx.doi.org/10.1016/j.apcatb.2012.12.008

increase of the activity [19]. And the improvement of lattice oxygen mobility of manganese oxides sharply increases the reactivity of Mn–Ag catalysts for CO oxidation [20].

A combination of Ag and Mn seems to be an important contributing factor to the reactivity [19–24]. However the details of application in toluene catalytic oxidation are not yet available. It has been proved that high dispersion of MnO_x on the surface are beneficial for the catalytic oxidation [15], and the mesoporous materials with high surface area, such as SBA-15 silica, can afford metal oxides with high dispersion [25,26]. It has been reported that SBA-15 can make the deactivation by carbonaceous formation and pore blocking less pronounced in toluene catalytic reaction [27]. Thus in the present work, we report the development of manganese oxide supported on SBA-15 with silver species for the toluene oxidation. The structure properties of Ag-Mn/SBA-15 and the link between structure and the catalytic performance of toluene oxidation are systemically investigated.

2. Experimental

2.1. Catalyst preparation

SBA-15 was synthesized by using triblock copolymer P123 ($EO_{20}PO_{70}EO_{20}$) as a structure directing agent according to the procedure reported by Zhao et al. [25], and Ag-Mn/SBA-15 catalysts were prepared by incipient wetness impregnation method. It involved the impregnation of SBA-15 with proper amount of $Mn(NO_3)_2$ and $AgNO_3$. The as-synthesized sample was dried overnight at RT, and then heated at 100 °C for 12 h. The whole metal weight loading on the support was fixed to a value of 16 wt% according to our experiment results. The Ag/Mn molar ratio was varied and the prepared catalysts were denoted as Ag-Mn/SBA-15(a:b), where a:b meant the Ag/Mn molar ratio.

The pure manganese oxide used in this paper was prepared by calcination of $Mn(NO_3)_2{\cdot}4H_2O$ at 500 °C for 2 h.

2.2. Catalytic test

Catalytic activity tests were carried out in a continuous flow reactor at atmospheric pressure. Toluene was introduced in a reactor, with the aid of a controlled Ar flow passing through the saturator. The concentration of toluene was 2500 ppm around, which was controlled by the temperature of the saturator and mixed with another O_2/Ar stream. The flow rate of gas mixture through the reactor was 50 ml/min gas flow. To ensure the constant concentration of toluene during the reaction process, the concentration of toluene was always measured before, in the middle and the end of the test by a by-pass valve. All lines were heated sufficiently at 120 °C to prevent the adsorption and condensation of the reactant and product in the tubes. Prior to all catalytic tests, the samples were pretreated in a flowing 20% O_2/Ar mixture at 500 °C for 2 h, and followed by cooling down to the reaction temperature in the Ar. The temperature, measured with a coaxial thermocouple, was varied between 200 °C and 350 °C. Each reaction temperature was kept half an hour until reaching the steady state of system and the data reported at the reaction temperature was the average value of at least three measurements. When the complete conversion for toluene oxidation was obtained, the temperature was kept for 48 h to test the reaction stability of the catalyst. The effluent gases were analyzed on-line at a given temperature by using gas chromatographs (Agilent 7890A) equipped with FID and TCD detectors for the quantitative analysis of the reactants and products. In the present work, the final products were CO_2 and H_2O under the experimental conditions. The conversion was calculated based on the toluene consumption.

2.3. Characterization of catalysts

Brunauer–Emmet–Teller (BET) surface areas of the samples were measured using N_2 physisorption at 77 K on a Quantachrome SI instrument. The elemental composition for Mn and Ag of the catalysts were analyzed using ion coupled plasma (ICP) atomic emission spectroscopy on a PerkinElmer Optima 2000DV spectrometer, and the results for the samples with different Ag:Mn molar ratios were as follows, 1:6, 1:3, 1:2, 1:1. Then the modified catalysts were denoted as Ag-Mn/SBA-15 (1:6), Ag-Mn/SBA-15 (1:3), Ag-Mn/SBA-15 (1:2) and Ag-Mn/SBA-15 (1:1). X-ray diffraction (XRD) patterns were obtained on Rigaku D/max-γb X-ray diffractometer using Cu-Kα radiation. Transmission electron microscopy (TEM) experiments were performed on a JEM-2000EX microscope with an operating voltage of 100 kV. UV–vis diffuse reflectance spectra were recorded in air on a SHIMADZU UV–2450 UV–vis spectrophotometer.

The XPS measurements were measured using an X-ray photoelectron spectrometer (AMICUS, Shimadzu) with a monochromatic X-ray source of Al Kα under ultra-high vacuum ($3–2 \times 10^{-6}$ Pa). The carbonaceous C 1s line (284.6 eV) was used as the reference to calibrate the binding energies. The deconvolution method of XPS spectra is fitted by Gaussian function.

The TPR measurements were performed on Quantachrom Automated Chemisorption Analyzer. A 50 mg of each sample was loaded into the reactor and purged with 30 ml/min of helium at 300 °C for 1 h to eliminate contaminants, and then cooled down to room temperature. The temperature was increased to 950 °C at a heating rate of 10 °C/min with flowing of 10% H_2/Ar. The temperature-programmed desorption (TPD) of oxygen was carried out using a quartz reactor connected to mass spectrometry. The samples were pretreated in oxygen at 500 °C for 2 h and cooled down in helium to room temperature. Subsequently, the catalysts were heated in helium to 950 °C at a rate of 5 °C/min.

In situ Fourier transform infrared (FTIR) experiments were carried out with Bruker Vertex 70. The pure catalyst powder was pressed into self-supporting disks and the temperature was measured by a thermocouple placed in close to the sample. Prior to adsorption experiment, the samples were pretreated in situ in He flow at 300 °C for 1 h and then cooled down to room temperature in He flow. After the saturation of toluene over samples at room temperature, the cell was purged with He to remove toluene in gas phase. Subsequently, the samples were heated in O_2, and the spectra were collected at different temperatures from room temperature to 260 °C.

3. Results and discussion

3.1. BET results

The specific surface area, pore volume and pore size of the catalysts are listed in Table 1. The surface area of Mn/SBA-15 sharply decreases to 518 m^2g^{-1} from 667 m^2g^{-1} for SBA-15. When the silver is loaded on the manganese oxide (Ag/Mn = 1:6), the surface area of catalysts declines to 465 m^2g^{-1}. However, it is interestingly found that the surface area shows an obvious increase (553 m^2g^{-1}) for Ag-Mn/SBA-15(1:3) compared with the Ag-Mn/SBA-15(1:6) catalyst. When the Ag/Mn molar ratio is further increased, a steady decrease in the surface area is exhibited. The pore volume and pore size of all supported catalysts are lower than the parent support, which might be resulted from the occupation of parts of Mn or Ag compounds into the pores of the support. Interestingly, the Ag-Mn/SBA-15(1:3) catalyst shows the largest pore volume among the studied catalysts. And the pore volume exhibits a decrease trend with the increase of the Ag/Mn ratio to 1:2 and 1:1, however the pore size for the latter two samples is slightly increased.

Table 1
Physical and chemical properties of different catalysts.

Samples	S_{BET} (m^2g^{-1})	V_{pore} (cm^3/g^{-1})	D_{pore} (nm)	Loading (wt%)[a]	Surface content (wt%)[b]	Ag/Mn[c]	Ag^+/Ag^0[d]	Mn^{4+}/Mn^{3+}[e]	O_{latt}/O_{surf}[f]	(β/α)[g]
SBA-15	667	0.82	5.66					–	–	–
Mn/SBA-15	519	0.62	4.75	16	16.1			1.32	2.00	0.35
Ag-Mn/SBA-15(1:6)	465	0.51	4.41	Mn:12.0 Ag:4.0	Mn_{surf}:8.22 Ag_{surf}:3.93	0.24	0.43	0.81	3.02	0.71
Ag-Mn/SBA-15(1:3)	553	0.75	5.21	Mn:9.6 Ag:6.4	Mn_{surf}:8.51 Ag_{surf}:6.52	0.39	0.73	0.32	3.78	2.20
Ag-Mn/SBA-15(1:2)	503	0.67	5.30	Mn:8.0 Ag:8.0	Mn_{surf}:7.82 Ag_{surf}:9.12	0.59	0.43	0.35	3.58	2.02
Ag-Mn/SBA-15(1:1)	467	0.61	5.54	Mn:5.4 Ag:10.6	Mn_{surf}:4.25 Ag_{surf}:8.09	0.95	0.55	0.64	2.39	9.68
Ag/SBA-15	402	0.47	5.61	16	13					

[a] The metal loading is obtained by ICP measurement.
[b] The surface metal loading is calculated from the XPS spectra.
[c] The surface Ag/Mn molar ratio is calculated from the XPS results.
[d] Ag^+/Ag^0 is calculated from the XPS results.
[e] Mn^{4+}/Mn^{3+} is calculated from the XPS results.
[f] O_{latt}/O_{surf} is calculated from the XPS results.
[g] β/α ratio is obtained from O_2-TPD results.

3.2. XRD patterns

Fig. 1(A) exhibits the low-angle X-ray diffraction patterns of SBA-15 and Ag-Mn/SBA-15(1:3). The (1 0 0), (1 1 0), (2 0 0) reflection peaks in the XRD pattern of SBA-15 associated with the hexagonal space group p6 mm is observed, indicating a well-ordered mesostructure [26]. The three reflection peaks for SBA-15, without the obvious shift, are still observed on Ag-Mn/SBA-15, which indicates that the loading of the Ag and Mn on the support has no influence on the well-ordered mesostructure of SBA-15. The intensity for low-angle XRD pattern of Ag-Mn/SBA-15(1:3), comparatively with the XRD pattern of SBA-15, is less pronounced which may be ascribed to X-ray absorption by Mn-species [28].

Fig. 1(B) shows the wide-angle XRD patterns of Ag-Mn/SBA-15, Mn/SBA-15 and Ag/SBA-15 catalysts. Several peaks with 2θ at 37.28°, 42.55°, and 56.54° are observed on the Mn/SBA-15, which can be ascribed to the presence of MnO_2 (JCPDS 72-1982). Ag (JCPDS 04-0783) can be found in the XRD pattern of Ag/SBA-15 catalyst. When Ag is introduced into Mn/SBA-15 catalyst, the peaks with 2θ at 37.28° and 56.54° are intensified. And the appearance of peaks with 2θ at 28.88°, 32.18°, 37.38°, 46.17° and 56.7° indicates the presence of $Ag_{1.8}Mn_8O_{16}$ (JCPDS 84-0873) together with MnO_2. With further increasing the Ag/Mn molar ratio to 1:3, peaks with 2θ at 28.88°, 37.38° are weakened and broadened. And meanwhile the peaks with 2θ at 32.18°, 46.17° and 56.54° disappear, which indicates the amount of $Ag_{1.8}Mn_8O_{16}$ and MnO_2 is decreased. Also new peaks with 2θ at 33.02°, 38.15° and 47.46° assigned to the Mn_2O_3 (JCPSD 71-0636) appear in the spectrum. Parts of MnO_2 are transformed into Mn_2O_3. When the Ag/Mn molar ratio is further increased to 1:2 and 1:1, all diffraction peaks decline to be nearly unobservable in XRD patterns.

3.3. TEM results

Fig. 2 shows the TEM images of the different catalysts. It clearly shows the well-ordered channel structure of the support, which is in good agreement with the XRD results (Fig. 1 (A)). Lots of silver particles can be observed on the Ag/SBA-15 catalyst, however, no such phenomenon can be observed on other catalysts. With the Ag addition from the ratio 1:6 to 1:3, more active compounds are finely dispersed on the surface of the support, and no obvious large particles are observed compared with Ag-Mn/SBA-15(1:6) catalyst, which induces the increase of the BET, pore volume and pore size. The compounds dispersed on the support should include MnO_x, Ag_xO, Ag or $AgMnO_x$ according to the EDX results. However, it is difficult to well distinguish these species separately. Further increasing the Ag/Mn ratio to 1:2 and 1:1, the high dispersion of the species on the support is observed, which is in well accord with

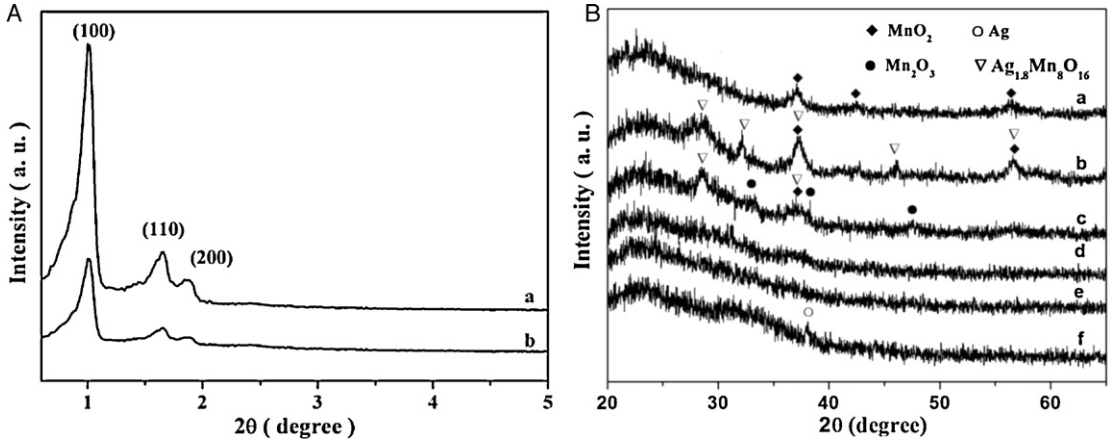

Fig. 1. (A) The low angle XRD patterns of SBA-15 (a) and Ag-Mn/SBA-15(1:3) catalysts (b); (B) the wide angle XRD patterns of (a) Mn/SBA-15, (b) Ag-Mn/SBA-15(1:6), (c) Ag-Mn/SBA-15(1:3), (d) Ag-Mn/SBA-15(1:2), (e) Ag-Mn/SBA-15(1:1) and (f) Ag/SBA-15 catalysts.

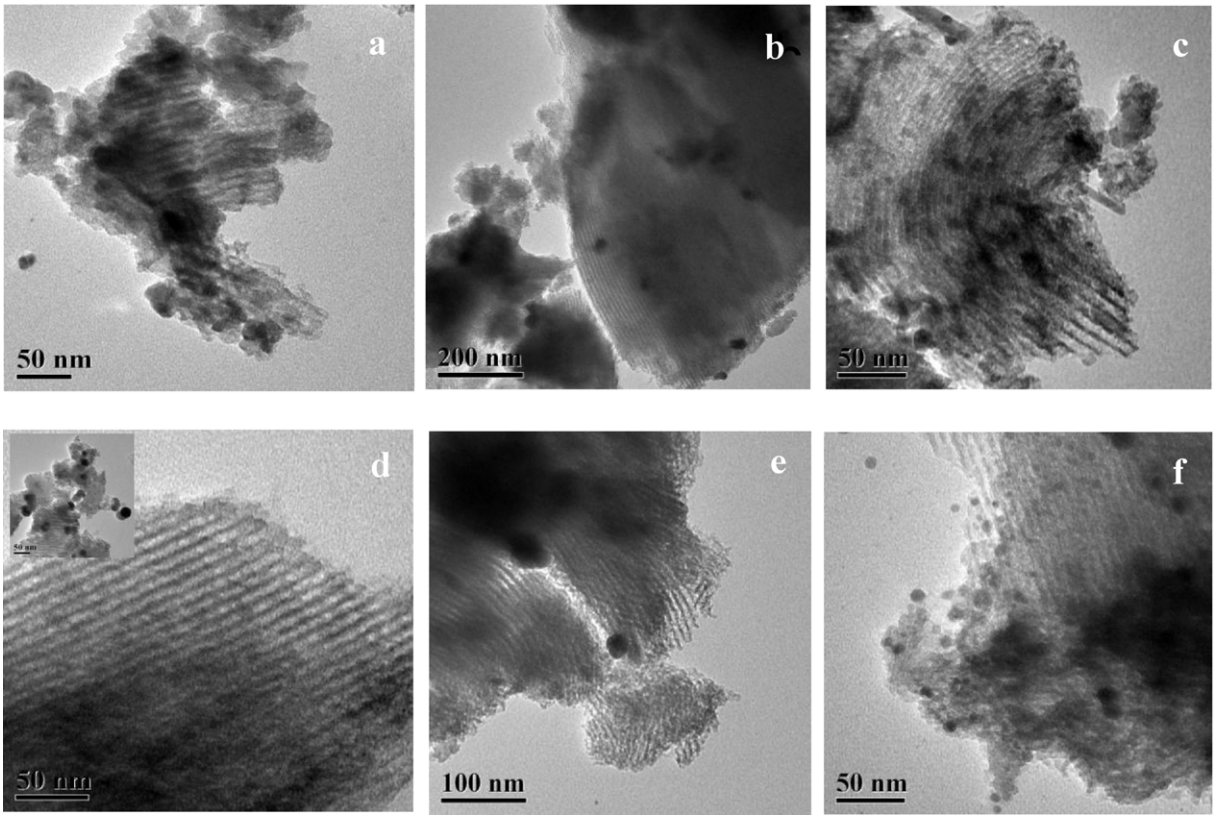

Fig. 2. TEM images of (a) Mn/SBA-15, (b) Ag-Mn/SBA-15(1/6), (c) Ag-Mn/SBA-15(1/3), (d) Ag-Mn/SBA-15(1/2), (e) Ag-Mn/SBA-15(1/1) and (f) Ag/SBA-15 catalysts.

the XRD results (Fig. 1B). The relative increase of the pore size indicates that these species are more easily dispersed on the surface not in the pore. However, a little large particle on the surface can be observed on the two samples, which might result in the decrease of the BET and pore volume and the diffusion limitations of the reactant gas.

3.4. UV–vis DRS

Fig. 3 shows the UV–vis diffuse reflectance spectroscopy (DRS) of Ag-Mn/SBA-15, Mn/SBA-15 and Ag/SBA-15 catalysts. All containing Mn samples exhibit a band at ca. 213 nm attributed to $O^{2-} \rightarrow Mn^{2+}$ charge transfer transition [29]. A wide and strong band is located between 300 and 700 nm for Mn/SBA-15. The band at 300–500 nm can be assigned to a mixture of Mn^{3+} and Mn^{4+} oxo species and that at 500–700 nm to Mn^{2+} [30,31], as shown in Table 2. Two adsorption bands can be observed at 219 and 404 nm for Ag/SBA-15, which are assigned to Ag^{+} and Ag [32]. For Ag-Mn/SBA-15(1:6) catalyst, the adsorption band at 500–700 nm declines slightly and the peak maximum moves to 408 nm. That is to say that the content of Mn^{3+} rises slightly at the expense of Mn^{2+} amount mainly. With further increasing the Ag/Mn ratio to 1:3, the intensity of the band at around 400–550 nm declines sharply, and meanwhile the band shifts to 373 nm. It means that the content of Mn^{3+} increases while that of Mn^{4+} decreases. The Ag-Mn/SBA-15(1:2) exhibits a similar pattern as Ag-Mn/SBA-15(1:3), and only the band slightly moves to higher wavelength. However, when the Ag/Mn molar ratio is increased to 1:1, the shift of the band to 414 nm and the slight enhancement of the band at ca. 500–700 nm are observed. This band shift may be due to the formation of Ag particles and (or) a slight increase of Mn^{4+} amount. Meanwhile the Mn^{2+} amount also is increased when the Ag/Mn ratio is increased to 1:1.

3.5. Surface chemical states of the Ag-Mn/SBA-15 catalysts

Characterization of chemical species located in the region near the catalyst surface is carried out by XPS. The deconvolution of Mn $2p_{3/2}$ signal is known to be useful to distinguish the states

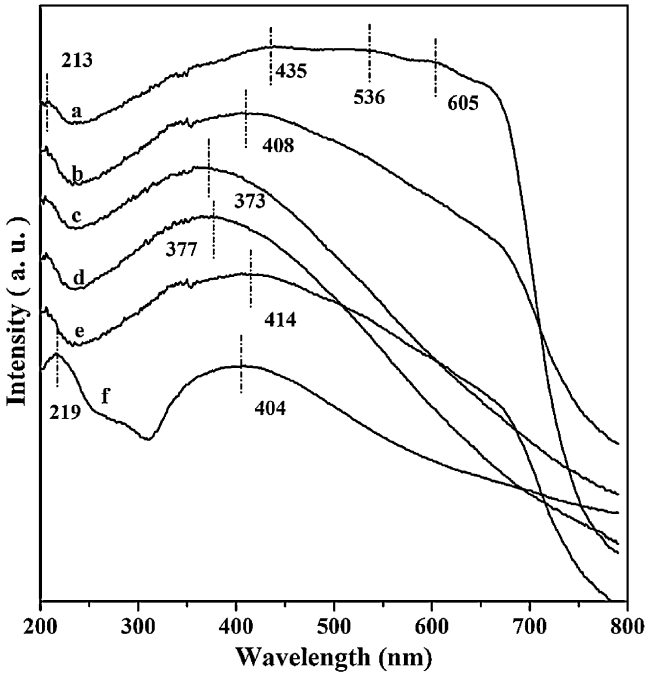

Fig. 3. Diffuse reflectance UV–vis spectra of (a) Mn/SBA-15, (b) Ag-Mn/SBA-15(1:6), (c) Ag-Mn/SBA-15(1:3), (d) Ag-Mn/SBA-15(1:2), (e) Ag-Mn/SBA-15(1:1) and (f) Ag/SBA-15 catalysts.

Table 2
Literature data on the charge-transfer and d–d transfer transitions of some compounds.

Compound	Mn^{n+}	λ_{max} (nm)	Assignment	Reference
MnO_2	Mn^{4+}	400–550	$O^{2-} \rightarrow Mn^{4+}$	[37–41]
Mn_2O_3	Mn^{3+}	340–370	$O^{2-} \rightarrow Mn^{3+}$	[40,41]
MnO	Mn^{2+}	500–600	$O^{2-} \rightarrow Mn^{2+}$	[41]
Mn/SBA-15	Mn^{3+}	435	$O^{2-} \rightarrow Mn^{3+}$	This study
	Mn^{4+}		$O^{2-} \rightarrow Mn^{4+}$	
	Mn^{2+}		$O^{2-} \rightarrow Mn^{2+}$	
Ag-Mn/SBA-15(1:6)	Mn^{3+}	408	$O^{2-} \rightarrow Mn^{4+}$	This study
	Mn^{4+}		$O^{2-} \rightarrow Mn^{3+}$	
Ag-Mn/SBA-15(1:3)	Mn^{3+} Mn^{4+}	373	$O^{2-} \rightarrow Mn^{4+} O^{2-} \rightarrow Mn^{3+}$	This study
Ag-Mn/SBA-15(1:2)	Mn^{3+}	377	$O^{2-} \rightarrow Mn^{4+}$	This study
	Mn^{4+}		$O^{2-} \rightarrow Mn^{3+}$	
Ag-Mn/SBA-15(1:1)	Mn^{4+}	414	$O^{2-} \rightarrow Mn^{4+}$	This study
	Mn^{3+}		$O^{2-} \rightarrow Mn^{3+}$	
	Mn^{2+}		$O^{2-} \rightarrow Mn^{2+}$	

of $Mn^{\delta+}$ and the results are recorded in Fig. 4. The binding energies of Mn $2p_{3/2}$ in the intervals 639.9–640.3 eV, 640.5–641.5 eV and 642.0–642.5 eV can be ascribed to the presence of Mn^{2+}, Mn^{3+} and Mn^{4+} ions, respectively [33]. Then different manganese states are assigned and the detail information is recorded in Table 1. It can be observed that the actual ratio of Mn^{4+}/Mn^{3+} is 1.31 on the surface of Mn/SBA-15. The MnO_2 is main manganese oxide, which result is consistent with the XRD and UV–Vis results. The ratio value decreases steadily as the content of Ag/Mn is increased to 1/3, and the ratio of Mn^{4+}/Mn^{3+} is only 0.32. But the Mn^{4+}/Mn^{3+} ratio is obviously increased for Ag-Mn/SBA-15(1:1) catalyst. More Mn^{3+} forms on the surface of the Ag-Mn/SBA-15(1:3) catalyst, and the ratio decreases with the further increase of the silver loading in the Mn based catalyst.

The O1s spectra exhibit two peaks and the peak at lower binding energy (529.4–530.0 eV) represents lattice oxygen (O_{latt}), whereas that at 531.3–532.3 eV corresponds to the surface-adsorbed oxygen such as O_2^{2-} or O^- corresponding a hydroxyl-like group (O_{surf}) [4,33]. For Mn/SBA-15 sample, the binding energy for lattice oxygen and surface oxygen is 529.97 eV and 531.23 eV, respectively. It is found that the binding energy shifts to 530.38 eV and 532.01 eV for Ag-Mn/SBA-15(1:3) catalyst. The increase in the binding energy after the addition of Ag seems to be the evidence of the presence of a defect in manganese. The ratios of O_{latt} to O_{surf} for different catalysts are also listed in Table 1. Specifically, the value of O_{latt}/O_{surf} increases steadily as Ag/Mn is increased to 1/3, while that declines in Ag-Mn/SBA-15(1:1), which is well connected with the trend in the reactivity of catalysts in the toluene conversion.

In order to well investigate the chemical state of the silver species on Ag-Mn/SBA-15 catalysts, the Ag 3d photoelectron spectra of different catalysts are also shown in Fig. 4. The deconvolution of Ag $3d_{2/5}$ signal shows that Ag^0 (368.35–368.55 eV) and Ag^+ (367.45–367.85 eV) species are coexisted on the Ag-Mn/SBA-15 catalysts (not show here) [34]. However the obvious shift for the binding energy of the main Ag $3d_{5/2}$ peak from 368.3 eV to 367.6 eV can be observed on the Ag-Mn/SBA-15 (1:3) catalyst, which indicates more oxidized silver species form on the catalyst easily. The Ag^+/Ag^0 ratio shown in Table 1 gives the strong evidence for it, and the content of the former increases with the Ag/Mn ratio to 1:3, which is an indication of the strong interactions between silver and MnO_x. The better dispersion for Mn and Ag species on the surface of the support can be found on Ag-Mn/SBA-15(1:3 and 1:2) catalysts from Table 1. Interestingly, the similar surface and bulk Ag/Mn molar ratio can be found on the Ag-Mn/SBA (1:3, 1:2 and 1:1) catalysts. Therefore, the Ag/Mn molar ratio shows the significant effects on the molar ratios of O_{latt}/O_{surf} and Mn^{4+}/Mn^{3+} through

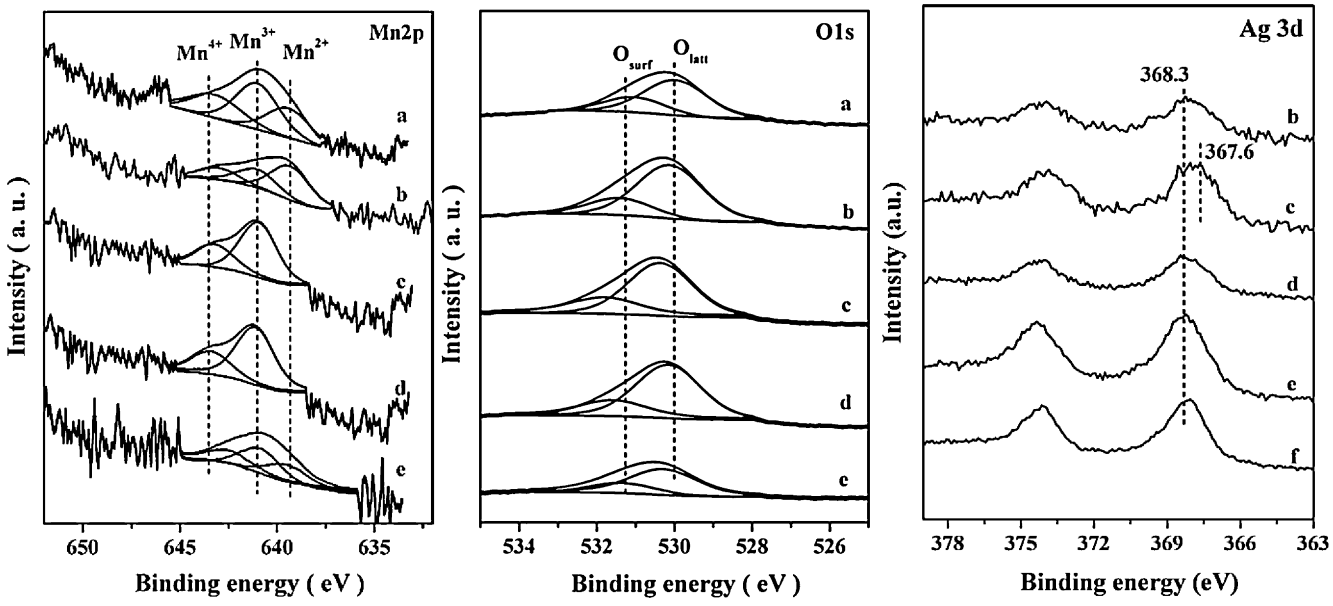

Fig. 4. XPS spectra of Mn2p, O1s and Ag3d of (a) Mn/SBA-15, (b) Ag-Mn/SBA-15(1/6), (c) Ag-Mn/SBA-15(1/3), (d) Ag-Mn/SBA-15(1/2), (e) Ag-Mn/SBA-15(1/1) and (f) Ag/SBA-15 catalysts.

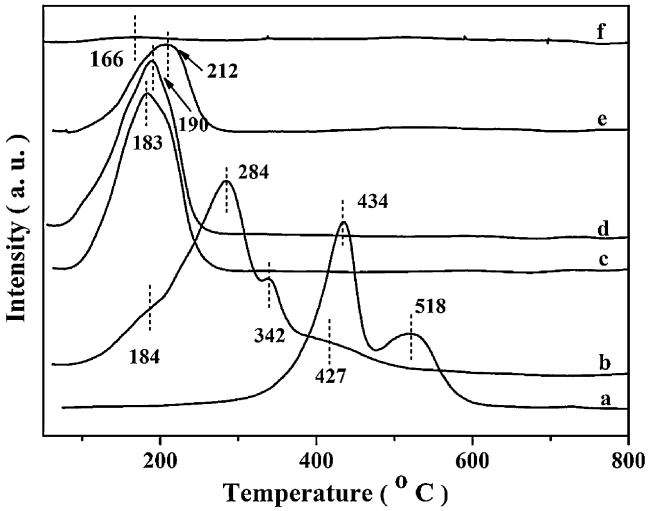

Fig. 5. H_2-TPR profiles of (a) Mn/SBA-15, (b) Ag-Mn/SBA-15(1:6), (c) Ag-Mn/SBA-15(1:3), (d) Ag-Mn/SBA-15(1:2), (e) Ag-Mn/SBA-15(1:1) and (f) Ag/SBA-15 catalysts.

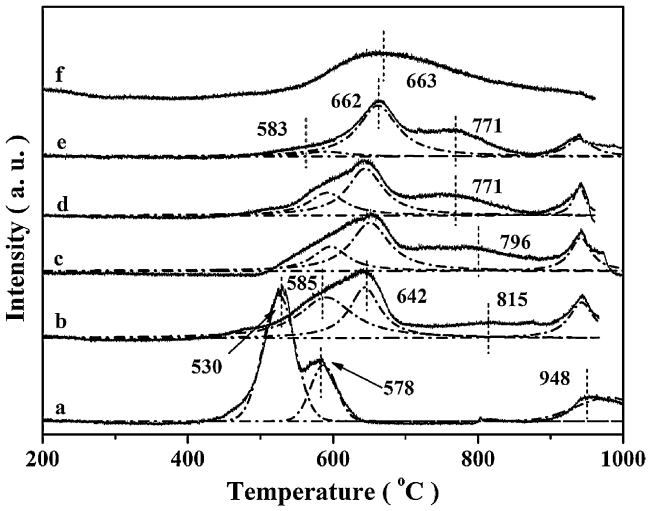

Fig. 6. O_2-TPD profiles of (a) Mn/SBA-15, (b) Ag-Mn/SBA-15(1:6), (c) Ag-Mn/SBA-15(1:3), (d) Ag-Mn/SBA-15(1:2), (e) Ag-Mn/SBA-15(1:1) and (f) Ag/SBA-15 catalysts.

the interaction between silver and MnO_x, which will influence the catalytic activity of Ag-Mn/SBA-15 catalysts for toluene oxidation.

3.6. TPR and O_2-TPD results

Fig. 5 presents the TPR profiles of the Mn/SBA-15, Ag/SBA-15, and Ag-Mn/SBA-15 catalysts. Reduction of Mn/SBA-15 takes place in the form of two overlapped peaks at 434 °C and 518 °C. The peak at low temperature can be assigned to the reduction of MnO_2 to Mn_3O_4, and the other one to the reduction of Mn_3O_4 to MnO [33,35,36]. Due to the larger negative value of its reduction potential, the reduction of MnO to form Mn metal is not observed even to a reduction temperature of 800 °C [36]. For Ag/SBA-15, a negligible reduction peak can be observed at 166 °C, which is assigned to the reduction of Ag_2O to Ag [37].

For all Ag-Mn/SBA-15 catalysts, all reduction peaks shift to lower temperatures considerably in comparison with Mn/SBA-15 catalyst. Specifically, the two peaks sharply shift to 284 and 342 °C from 434 °C and 518 °C in the reduction profile of Ag-Mn/SBA-15(1:6), respectively. Also a small shoulder peak and a weak peak appear at 184 °C and 427 °C. Meanwhile, the main reduction peak becomes more intensive than that of Mn/SBA-15, while the second peak shrinks to a shoulder peak.

As the content of Ag is further increased, only one reduction peak at 183 °C in the profile of Ag-Mn/SBA-15(1:3) is observed. Then the peak shifts to 190 °C for Ag-Mn/SBA-15(1:2) and finally to 212 °C for Ag-Mn/SBA-15(1:1). Though the reduction peak located at 200 °C around approaches that of Ag_2O, the intensity of the peak is far larger than that of Ag_2O. Thus, it can be assigned to the manganese oxides being directly reduced to MnO at low temperature due to the effect of Ag. The differences in reducibility of different Ag-Mn/SBA-15 catalysts can be attributed to changes in the composition of catalysts with various Ag/Mn molar ratios. Also it is noteworthy that the intensity of the peak at ca. 200 °C is enhanced gradually as the Ag/Mn molar ratio is increased from 0 to 1:3. Then the band declines in intensity for Ag-Mn/SBA-15(1:2) and Ag-Mn/SBA-15(1:1) steadily. Thus an appropriate Ag/Mn molar ratio will lead to the direct reduction of the abundant of manganese oxides at low temperatures.

Fig. 6 records the O_2-TPD profiles of Ag-Mn/SBA-15 with different Ag/Mn molar ratios. The strong desorption peak at 530 °C (α peak) for Mn/SBA-15 catalyst is assigned to the desorption peak of lattice oxygen from MnO_2 to produce Mn_2O_3 [24]. The other two peaks at 578 °C (β peak) and 948 °C (γ peak) in the spectrum belong to the desorption peak of the lattice oxygen of Mn_2O_3 to form Mn_3O_4 and MnO [24,38], respectively. A broad peak at 663 °C can be observed in the pattern of Ag/SBA-15, which can be assigned to oxygen desorption from Ag subsurface [39]. When Ag is introduced into the samples, no obvious change for desorption peak at 948 °C is found. However the desorption peak at 400–650 °C shifts to higher temperature, and becomes broad and irregular. This may be related with the facts that Ag disturbs the structure of manganese oxides and the defective sites forms in the sample. The O_2-TPD patterns of Mn/SBA-15 with different Mn loadings are recorded in Fig. 7. Only changes in intensity of oxygen desorption peaks can be observed, and no obvious shift is found. Thus, the peak shift for the Ag-Mn/SBA-15 should be ascribed to the interaction between Ag and Mn species.

The further curve-fitting results for the O_2-TPD have been obviously exhibited in Fig. 6. For Ag-Mn/SBA-15(1:6), it is apparent that oxygen desorption peaks of manganese oxides shift to 585 and 642 °C. Meanwhile the intensity of the peak at 585 °C declines sharply while the intensity of that at 642 °C goes up slightly. Also a weak peak at 815 °C appears in the spectrum. Combined with results of XRD and DRS, the peak at 585 °C can be assigned to oxygen

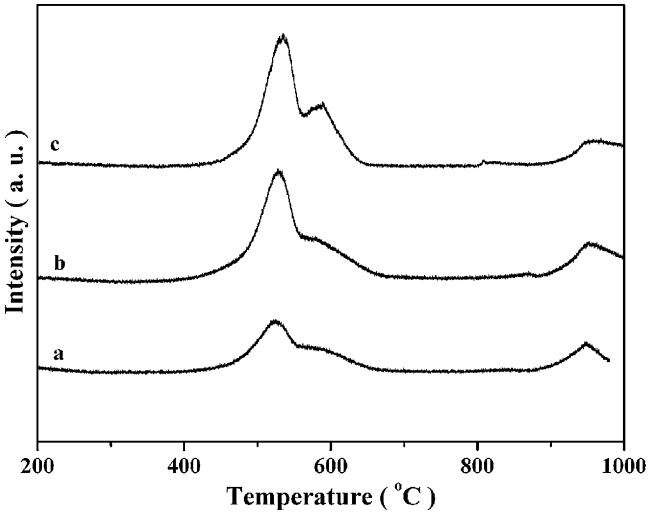

Fig. 7. O_2-TPD profiles of Mn/SBA-15 catalysts with different Mn loadings (a): 4 wt %, (b): 8 wt% and (c): 12 wt%.

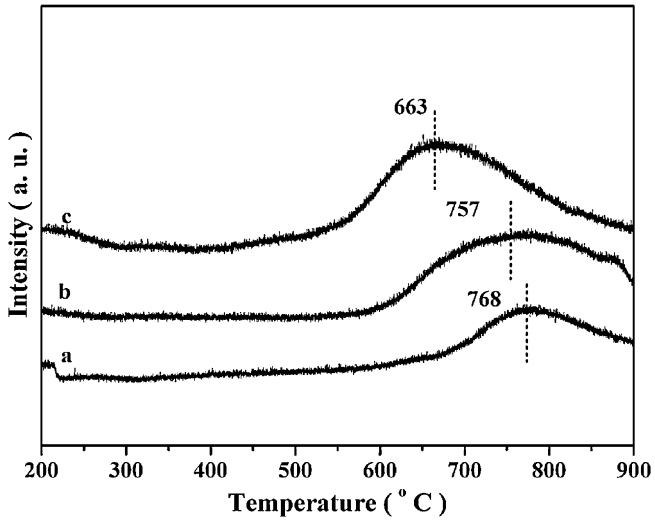

Fig. 8. O_2-TPD profiles of Ag/SBA-15 catalysts with different Ag loadings. (a): 4 wt%, (b): 8 wt% and (c): 10.6 wt%.

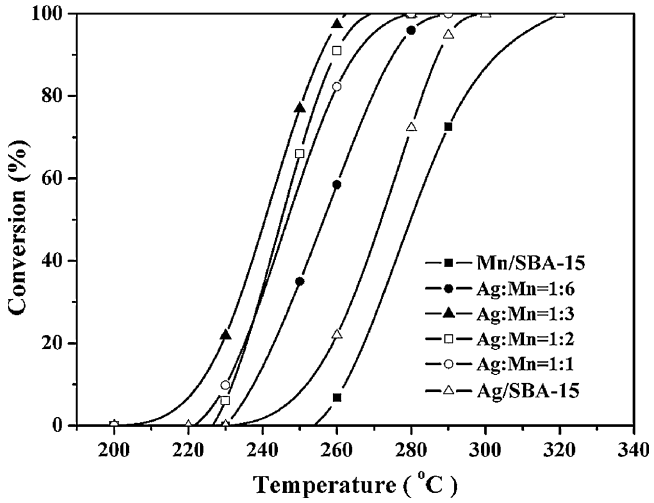

Fig. 9. Catalytic performances of Ag-Mn/SBA-15 catalysts with different Ag/Mn molar ratios for toluene oxidation.

desorption of MnO_2 and that at 642 °C can be attributed to oxygen desorption of Mn_2O_3 and the defective $Ag_{1.8}Mn_8O_{16}$ [36,40].

The area ratio for β/α on different sample is exhibited in Table 1, and it can be observed that the area ratio is increased with the increase of Ag/Mn to 1:3, then decreases. An oppositely sharp increase for the ratio of the β/α on Ag-Mn/SBA-15(1:1) is observed. The more amount of oxygen from Mn_2O_3 and (or) the defective $Ag_{1.8}Mn_8O_{16}$ is desorbed on the Ag modified Mn based catalysts. That is to say that the amount of MnO_2 declines with the further increase of silver loading, while that of Mn_2O_3 and $Ag_{1.8}Mn_8O_{16}$ rises gradually. It has been known from the results of the DRS and XPS that the amount of Mn^{4+} has started to be enhanced when the Ag/Mn molar ratio is increased to 1:1, thus the unobservable α peak for O_2-TPD might be due to the low loading of MnO_x or some unclear reason.

The intensity of the desorption peak in 700–850 °C range increases progressively and the peak shifts to lower temperature gradually from 815 to 663 °C with the silver loading. It has been known that the desorption peak will shift to lower temperature with the increase of silver loading on the Ag/SBA-15, as shown in Fig. 8. Thus it is reasonable to suggest that the peak in 700–850 °C range on Ag-Mn/SBA-15 catalysts is assigned to oxygen desorption from Ag subsurface. Also, it should be noted that the area for oxygen desorption in 700–850 °C range on Ag-Mn/SBA-15 is smaller than that on Ag/SBA-15 with the same amount of Ag, which might result from the fact that parts of Ag enter into MnO_x to form $Ag_{1.8}Mn_8O_{16}$.

3.7. Catalytic performance

The catalytic performances of Mn/SBA-15, Ag/SBA-15 and Ag-Mn/SBA-15 are evaluated in the toluene catalytic oxidation and the results are presented in Fig. 9. It is found that the doping of silver to Mn/SBA-15 significantly influence the activity for toluene oxidation of the catalyst, and the catalytic performance of Ag-Mn/SBA-15 strongly depends on the Ag/Mn molar ratio. The Ag-Mn/SBA-15(1:3) catalyst shows the best catalytic activity for toluene oxidation, with the complete toluene conversion at 260 °C, which is 60 °C lower than that of Mn/SBA-15. Specifically, the following performance trend is observed: Ag-Mn/SBA-15(1:3) (260 °C) > Ag-Mn/SBA-15(1:2) (270 °C) > Ag-Mn/SBA-15(1:1) (280 °C) > Ag-Mn/SBA-15(1:1) (290 °C) > Ag/SBA-15 (300 °C) > Mn/SBA-15 (320 °C).

Table 3 shows the comparison of catalytic performance of the toluene oxidation over different catalysts, including Ag-Mn/SBA-15(1:3), pure manganese oxides, other Mn-based catalysts and noble metal catalysts reported in the references. It is found that the catalytic activity for toluene oxidation over Mn/SBA-15 is higher than pure MnO_x. Also Ag-Mn/SBA-15(1:3) exhibits much higher reactivity than Ag/MnO_x. Thus it is reasonable to suggest that SBA-15 silica shows a significant promotion effect for the activity of MnO_x based catalysts, which should be related with the higher dispersion of manganese oxide on the surface. Also it can be noted that the performance of Ag-Mn/SBA-15 catalyst is comparable or even superior to that of Mn mixed catalysts with other elements and some noble catalysts.

The reaction stability for toluene oxidation with the time over different Ag-Mn catalysts have also been tested in the experiments, and the result for the Ag-Mn/SBA-15 (1:3) catalyst is shown in Fig. 10. The catalyst shows good reaction stability for toluene oxidation in 48 h, and the conversion is always remained above 99% at 260 °C. Other Ag-Mn/SBA-15 catalysts also show the similar results at a certain temperature in the studied period (not shown here).

It is noteworthy that no other by-product (such as CO) is detected in the activity test, and the final single carbon-containing product of toluene oxidation was CO_2. Only a small amount of

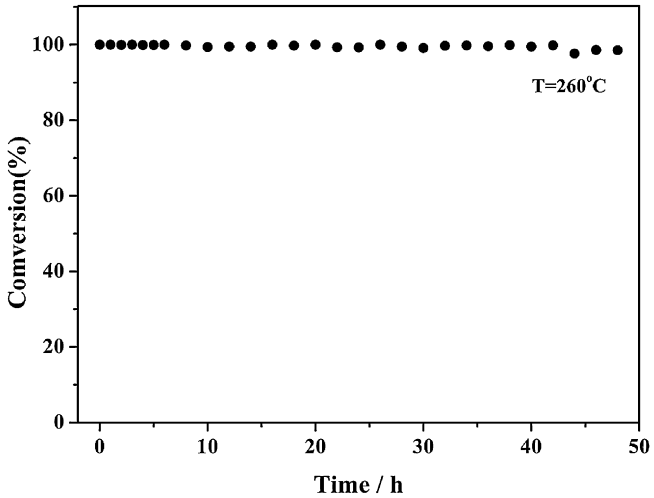

Fig. 10. Reaction stability with time for toluene oxidation over Ag-Mn/SBA-15(1:3) catalyst.

Table 3
The catalytic activity of various catalysts for toluene oxidation.

Catalysts	Activity (°C)				References
	T_{50}	T_{80}	T_{90}	T_{100}	
Ag-Mn/SBA-15(1:3)	240	250	255	260	This study
Mn/SBA-15	280	295	300	320	This study
MnO_x (Mn_2O_3, MnO_2)			345		This study
Ag/MnO_x			280		This study
MnO_2	340		375		[4]
Mn_2O_3	280		295		[4]
Mn_3O_4	245		270		[4]
$Mn_{0.5}Ce_{0.5}$				260	[17]
MnFe mixed oxide		293–307			[41]
Mn-Cu/MCM-41				>350	[42]
4 wt%Au/hydrotalcite	240				[43]
2.13wt%Pt-2.10wt%Au/ZnO/Al_2O_3	178–278	182–288			[44]
Pd/Beta	226		245		[45]
Pd/SBA-15	261		292		
Pd/MCM-48	267		301		
Pd/Co_3AlO			230–320		[46]

T_{50}, T_{80}, T_{90} and T_{100} (°C): the value of the temperature at conversion approaches 50%, 80%, 90%, 100% respectively
Reaction conditions: This study toluene concentration (*C*), 2500 ppm; flow rate (*F*), 50 ml/min; catalyst weight (CW), 0.2 g; gas hourly space velocity (GHSV), 15,000 h^{-1}.
[4] *C*, 1000 ppm; *F*, 100 ml/min; W, 0.4 g
[17] *C*, 600 ppm; *F*, 50 ml/min; W, 0.06 g;
[41] *F*, 100 ml/min; CW, 0.3 g;
[42] *C*, 3500 ppm; *F*, 60 ml/min; W, 0.1 g;
[43] *C*, 1000 ppm; *F*, 33.33 ml/min; CW, 0.1 g;
[44] *C*, 1.8 mol%; *F*, 40 ml/min; CW, 0.1 g;
[45] *C*, 650 ppm; CW, 0.3 g; GHSV, 26,000 h^{-1};
[46] *C*, 0.08 vol.%; *F*, 300 ml/min; CW, 0.6 g; GHSV, 30,000 h^{-1}.

intermediate species is detected by GC at low temperature during the activity test, and then the intermediate species is ultimately eliminated at 240 °C, which will be further investigated in the following in situ FTIR experiment.

It has been known that the oxidation of organic molecules with manganese oxide catalysts may involve a Mars–van Krevelen type mechanism. Lattice oxygen of the catalyst can be consumed by reaction with the VOCs and then be replenished by oxygen from the air stream [47–49]. Thus, lattice oxygen of manganese oxides can be of great importance in the catalytic oxidation of toluene. When silver is added into the catalyst, $Ag_{1.8}Mn_8O_{16}$ forms in Ag-Mn/SBA-15(1:6). The mixed silver manganese phase is of high reactivity in the catalytic oxidation. There exists surface electron exchange interactions between Mn^{3+} and Mn^{4+} existing in Ag-Mn mixed phase [40]. The d–d electron exchange interaction between closely coupled pairs of manganese atoms in different oxidation states facilitates the electronic mobility across the surface.

With the increase of the Ag/Mn molar ratio to 1:3, more Ag^+ species are generated, which enhances the interaction between Ag and Mn species, and more oxygen vacancies might be present on the supported silver catalyst. The Ag/Mn ratio shows a significant effects on the molar ratios of lattice oxygen to surface adsorbed oxygen and the surface Mn^{4+} to Mn^{3+} on the Ag-Mn/SB-15 catalysts through the interaction between silver and MnO_x. Part of MnO_2 is mainly transformed into Mn_2O_3, and the presence of MnO_2, Mn_2O_3 combined with $Ag_{1.8}Mn_8O_{16}$ facilitates the oxygen mobility and the activation of oxygen in the feed stream, promoting the redox property of Ag-Mn/SBA-15(1:3) and resulting in excellent reactivity [50–52]. MnO_2 would release oxygen to form Mn_2O_3 and the latter can get oxygen to activate oxygen in the air. The oxygen located between MnO_x and $MnCeO_x$ is of high mobility and is critical to catalytic combustion of chlorobenzene [33]. XPS results also suggest the presence of the defect in manganese, and these defective sites can be as the active centres in the catalytic reaction since the oxygen species of the defective oxides tends to be easily released and transferred, which enhance the reactivity of catalysts in oxidation of VOCs [53]. The decrease of the ratios of Mn^{3+}/Mn^{4+} and O_{latt}/O_{surf} on the catalysts results in the decline of the reducibility of the Ag-Mn/SBA-15(1:2) and Ag-Mn/SBA-15(1:1) catalysts, meanwhile the formation of a little larger particle on the surface of the support might influence the diffusion of reactant gas, and thus induces the decrease of the catalytic activity for toluene oxidation.

It is also find that the activities for toluene oxidation on the Ag-Mn/SBA (1:3, 1:2 and 1:1) catalysts are far high than that of the Ag-Mn/SBA (1:6) catalyst. Thus, we deduce that the homogeneous dispersion of Ag and Mn species on the surface might also play an important effect on the activity for toluene oxidation, which need a deep investigation in the near future.

3.8. In situ FTIR study

In situ FTIR technique is applied to reveal the preliminary information about the process of toluene catalytic oxidation over Ag-Mn catalysts, and the results are shown in Fig. 11. After toluene adsorption equilibrium reaches, the samples are treated by the He gas to remove toluene in the gas phase and parts of toluene weakly adsorbed on the surface of samples. The bands at 1394, 1452, 1496, and 1605 cm^{-1} are attributed to the toluene molecular (denoted as T), and the band at 1624 cm^{-1} is from the sample (denoted as S) in the spectrum of Mn/SBA-15 [Fig. 10A(a)]. By contrast, another two negligible bands at around 1643 and 1688 cm^{-1} appear in the spectra of Ag-Mn/SBA-15(1:3) [Fig. 11A(c)] and Ag-Mn/SBA-15(1:1) [Fig. 11d)]. The band at 1688 cm^{-1} has been assigned to the carbonyl vibration of the aldehyde group (C═O) [54,55] and that at 1643 cm^{-1} to molecular water (W) coordinated to the surface of the sample [56]. No such changes can be observed in the spectra of Ag-Mn/SBA-15(1:6) [Fig. 11A(b)].

When the catalysts are treated in O_2 heating flow, toluene adsorbed on Mn/SBA-15 is removed gradually with the increase of the heating temperature to 260 °C [Fig. 11B–E(a)], and no other bands can be found in the spectra. No toluene oxidation occurs under the reaction condition, whose result is similar with that obtained in the fixed bed reactor. By contrast, the intensity of the C═O band and water is enhanced slightly with the amount decrease of toluene molecular in the spectra of Ag-Mn/SBA-15(1:3) as the

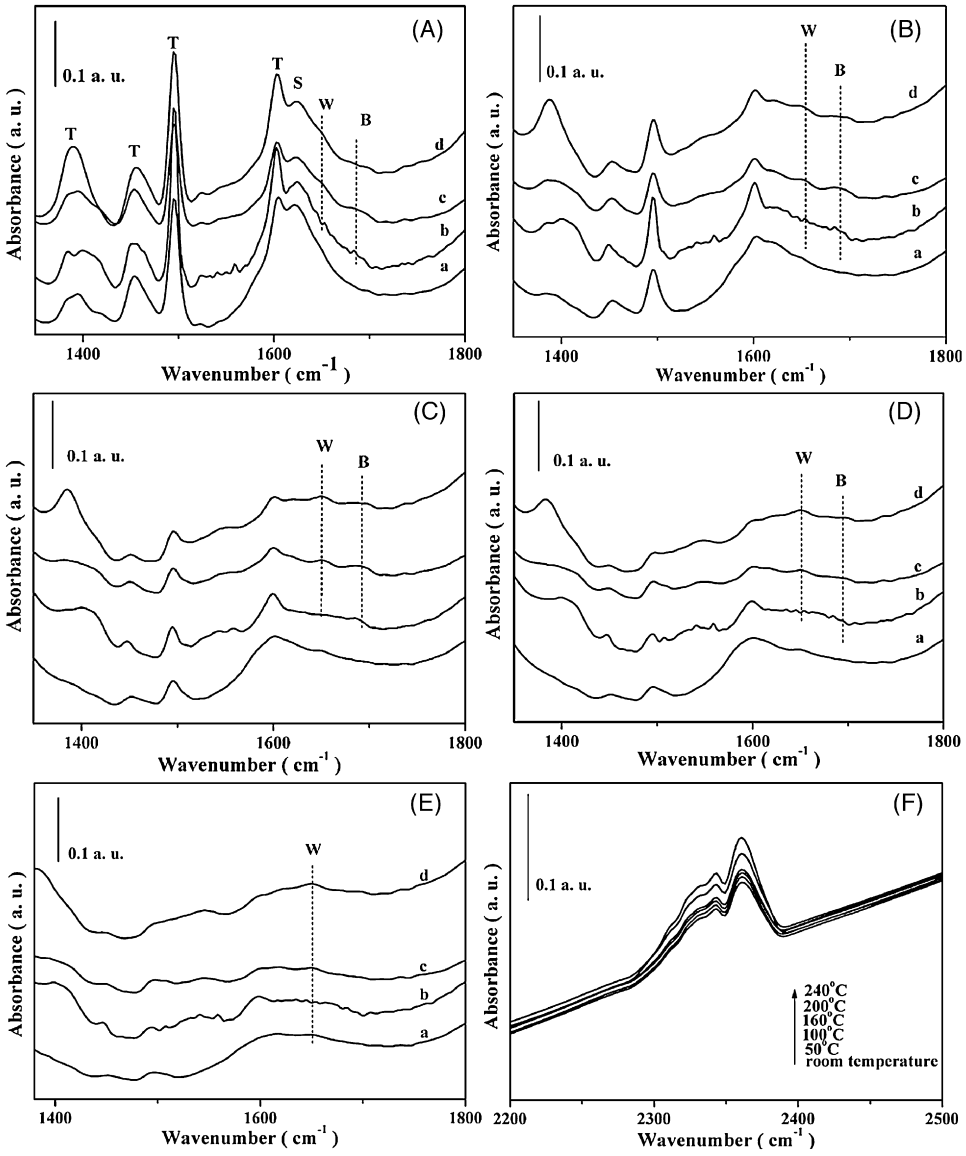

Fig. 11. FTIR spectra obtained from (a) Mn/SBA-15, (b) Ag-Mn/SBA-15(1:6), (c) Ag-Mn/SBA-15(1:3) and (d) Ag-Mn/SBA-15(1:1) in the region of 1350–1800 cm^{-1}, toluene adsorbed samples are treated in He gas phase (A). Then samples are heated in O_2 gas flow at (B) 100 °C, (C) 160 °C, (D) 240 °C, (E) 260 °C. The changes of carbon dioxide during the process of catalytic reaction over Ag-Mn/SBA-15(1:3) from room temperature to 260 °C are recorded in (F).

temperature is increased to 100 °C [Fig. 11B(c)]. The intermediate is accumulated on the surface of the catalyst. When the heating temperature is increased to 160 °C, the intensity of benzaldehyde tends to decline slightly [Fig. 11C(c)] and becomes nearly unobservable at 240–260 °C [Fig. 11D,E(c)]. Meanwhile, the intensity for the bands (2343, 2360 cm^{-1}) associated with CO_2 climbs up slightly with the temperature to 260 °C (Fig. 11F). The formed intermediate benzaldehyde can be gradually oxidized into carbon dioxide under the oxygen flow. The main products for the toluene oxidation on the Ag-Mn/SBA-15 catalyst are CO_2 and H_2O. It is reasonable to believe that the existence of the intermediate benzaldehyde combining with the GC observation though its intensity is weak. However, the relationship of intermediate formation with the Ag/Mn molar ratio is not clear from the present results.

Usually, the formation of benzaldehyde during the toluene oxidation involves essentially the high mobility of the lattice oxygen of oxides [57,58]. From in situ FTIR analysis, benzaldehyde is detected over Ag-Mn/SBA-15 at room temperature and is accumulated on the surface of catalysts in the heating O_2 flow. The accumulation of benzaldehyde may be ascribed to the easy mobility for lattice oxygen in the heating O_2 flow due to the replenishment of lattice oxygen from gas phase. Moreover it has been known from the XPS results that the ratio of the O_{latt}/O_{surf} is higher for Ag-Mn/SBA-15 compared with Mn/SBA-15. The Ag-Mn/SBA-15(1:3) catalyst with the highest O_{latt}/O_{surf} ration and relatively best oxygen reducibility exhibits highest activity for toluene oxidation. Thus it can be reasonably deduced that the formation of the intermediate benzaldehyde on Ag-Mn/SBA-15 catalysts should be closely related to the mobility of the lattice oxygen of Ag-Mn/SBA-15 catalysts.

4. Conclusions

The addition of Ag enhances the reactivity of Mn/SBA-15 greatly for toluene oxidation, and the Ag-Mn/SBA-15(1:3) shows the highest activity in the catalytic reaction. The appropriate Ag amount leads to the transformation of MnO_2 to Mn_2O_3 and the formation of defective $Ag_{1.8}Mn_8O_{16}$ phase. The ratios of Mn^{4+}/Mn^{3+} and O_{latt}/O_{surf} on the catalysts is enhanced gradually with the Ag/Mn ratio increasing to 1:3, and then decreases with the further

increasing of the silver loading. The presence of more Ag^+ on the Ag-Mn/SBA-15(1:3) catalyst enhances the interaction between Ag and Mn species. The coexistence of MnO_2, Mn_2O_3 and $Ag_{1.8}Mn_8O_{16}$ exhibits a good synergetic action, which promotes the reducibility of catalysts, the formation of abundant active lattice oxygen and thus the catalytic activity for toluene oxidation. The formation of abundant lattice oxygen on the Ag-Mn/SBA-15 catalysts will contribute to the formation of intermediate benzaldehyde species.

Acknowledgements

This work was supported financially by the Program for New Century Excellent Talents in University (NCET-09-0256) and the National High Technology Research and Development Program of China (863 Program) (No. 2009AA062604).

References

[1] J. Bedia, J.M. Rosas, J. Rodriguez-Mirasol, T. Cordero, Applied Catalysis B: Environmental 94 (2010) 8–18.
[2] L.F. Liotta, Applied Catalysis B: Environmental 100 (2010) 403–412.
[3] H.L. Tidahy, S. Siffert, F. Wyrwalski, J.F. Lamonier, A. Aboukais, Catalysis Today 119 (2007) 317–320.
[4] S.C. Kim, W.G. Shim, Applied Catalysis B: Environmental 98 (2010) 180–185.
[5] M. Baldi, V.S. Escribano, J.M.G. Amores, F. Milella, G. Busca, Applied Catalysis B: Environmental 17 (1998) 175–182.
[6] C. Lahousse, A. Bernier, P. Grange, B. Delmon, P. Papaefthimiou, T. Ioannides, X. Verykios, Journal of Catalysis 178 (1998) 214–225.
[7] J.Q. Torres, J.M. Giraudon, J.F. Lamonier, Catalysis Today 176 (2011) 277–280.
[8] J. Kugai, J.T. Miller, N. Guo, C.S. Song, Journal of Catalysis 277 (2010) 46–53.
[9] B. de Rivas, R. López-Fonseca, C. Jiménez-González, J.I. Gutiérrez-Ortiz, Journal of Catalysis 281 (2011) 88–97.
[10] F. Wyrwalski, J.M. Giraudon, J.F. Lamonier, Catalysis Letters 137 (2010) 141–149.
[11] V.P. Santos, M.F.R. Pereira, J.J.M. Órfão, J.L. Figueiredo, Applied Catalysis B: Environmental 99 (2010) 353–363.
[12] R.H. Wang, J.H. Li, Environmental Science and Technology 44 (2010) 4282–4287.
[13] V. Roche, L. Mazri, A. Boréave, M.H. Ta, L. Retailleau-Mevel, A. Giroir-Fendler, P. Vernoux, J.P. Deloume, Applied Catalysis A-General 385 (2010) 163–169.
[14] Y.S. Wu, Y.X. Zhang, M. Liu, Z.C. Ma, Catalysis Today 153 (2010) 170–175.
[15] R. Craciun, B. Nentwick, K. Hadjiivanov, H. Knözinger, Applied Catalysis A-General 243 (2003) 67–79.
[16] S. Imamura, N. Shono, A. Okamoto, S. Ishida, Applied Catalysis A-General 142 (1996) 279–288.
[17] D. Delimaris, T. Ioannides, Applied Catalysis B: Environmental 84 (2008) 303–312.
[18] M.R. Morales, B.P. Barbero, L.E. Cadus, Fuel 87 (2008) 1177–1186.
[19] W. Gac, G. Giecko, S. Pasieczna-Patkowska, T. Borowiecki, L. Kępiński, Catalysis Today 137 (2008) 397–402.
[20] A. Machocki, T. Ioannides, B. Stasinsk, W. Gac, G. Avgouropoulos, D. Delimaris, W. Grzegorczyk, S. Pasieczna, Journal of Catalysis 227 (2004) 282–296.
[21] Q. Ye, J.S. Zhao, F.F. Huo, J. Wang, S.Y. Cheng, T.F. Kang, H.X. Dai, Catalysis Today 175 (2011) 603–609.
[22] R. Xu, X. Wang, D.S. Wang, K.B. Zhou, Y.D. Li, Journal of Catalysis 237 (2006) 426–430.
[23] J.L. Chen, J. Li, H.J. Li, X.M. Huang, W.J. Shen, Microporous and Mesoporous Materials 116 (2008) 586–592.
[24] M.F. Luo, X.X. Yuan, X.M. Zheng, Applied Catalysis A-General 175 (1998) 121–129.
[25] D.Y. Zhao, J.L. Feng, Q.S. Huo, N. Melosh, G.H. Fredrickson, B.F. Chmelka, G.D. Stucky, Science 279 (1998) 548–552.
[26] T. Tsoncheva, J. Rosenholm, M. Linden, F. Kleitz, M. Tiemann, L. Ivanova, M. Dimitrov, D. Paneva, I. Mitov, C. Minchev, Microporous and Mesoporous Materials 112 (2008) 327–337.
[27] K. Bendahou, L. Cherif, S. Siffert, H.L. Tidahy, H. Benaïss, A. Aboukaïs, Applied Catalysis A-General 351 (2008) 82–87.
[28] W.P. Zhang, C.I. Ratcliffe, I.L. Moudrakovski, J.S. Tse, C.Y. Mou, J.A. Ripmeester, Microporous and Mesoporous Materials 79 (2005) 195–203.
[29] N. Stamatis, K. Goundani, J. Vakros, K. Bourikas, Ch. Kordulis, Applied Catalysis A 325 (2007) 322–327.
[30] L. Lamaita, M.A. Peluso, J.E. Sambeth, H.J. Thomas, Applied Catalysis B: Environmental 61 (2005) 114–119.
[31] S. Velu, N. Shah, T.M. Joythi, S. Sivasanker, Microporous and Mesoporous Materials 33 (1999) 61–75.
[32] N. Bogdanchikova, F.C. Meunier, M. Avalos-Borja, J.P. Breen, A. Pestryakov, Applied Catalysis B: Environmental 36 (2002) 287–297.
[33] Y. Dai, X.Y. Wang, Q.G. Dai, D. Li, Applied Catalysis B: Environmental 111–112 (2012) 141–149.
[34] P.H. Citrin, C.K. Wertheim, T. Baer, Physical Review B 27 (1983) 3160–3175.
[35] J. Carnö, M. Ferrandon, E. Björnbom, S. Järås, Applied Catalysis A-General 155 (1997) 265–281.
[36] J. Trawczyński, B. Bielak, W. Mišta, Applied Catalysis B: Environmental 55 (2005) 277–285.
[37] D. Chen, Z.P. Qu, S.J. Shen, X.Y. Li, Y. Shi, Y. Wang, Q. Fu, J.J. Wu, Catalysis Today 175 (2011) 338–345.
[38] S.T. Xing, C. Hu, J.H. Qu, H. He, M. Yang, Environmental Science and Technology 42 (2008) 3363–3368.
[39] G.I.N. Waterhouse, G.A. Bowmake, J.B. Metson, Applied Surface Science 214 (2003) 36–51.
[40] X. Wang, Y.C. Xie, New Journal of Chemistry 25 (2001) 964–969.
[41] F.G. Durán, B.P. Barbero, L.E. Cadús, C. Rojas, M.A. Centeno, J.A. Odriozola, Applied Catalysis B: Environmental 92 (2009) 194–201.
[42] W.B. Li, M. Zhuang, J.X. Wang, Catalysis Today 137 (2008) 340–344.
[43] E. Genty, R. Cousin, C. Gennequin, S. Capelle, A. Aboukaïs, S. Siffert, Catalysis Today 176 (2011) 116–119.
[44] K.J. Kim, H.G. Ahn, Applied Catalysis B: Environmental 91 (2009) 308–379.
[45] C. He, J.J. Li, J. Cheng, L.D. Li, P. Li, Z.P. Hao, Z.P. Xu, Industrial & Engineering Chemistry Research 48 (2009) 6930–6936.
[46] P. Li, C. He, J. Cheng, C.Y. Ma, B.J. Dou, Z.P. Hao, Applied Catalysis B: Environmental 101 (2011) 570–579.
[47] J. Luo, Q.H. Zhang, J. Garcia-Martinez, S.L. Suib, Journal of the American Chemical Society 130 (2008) 3198–3207.
[48] M. Baldi, E. Finocchio, F. Milella, G. Busca, Applied Catalysis B: Environmental 16 (1998) 43–51.
[49] C. Cellier, V. Ruaux, C. Lahousse, P. Grange, E.M. Gaigneaux, Catalysis Today 117 (2006) 350–355.
[50] G.S. Qi, R.T. Yang, R. Chang, Applied Catalysis B: Environmental 51 (2004) 93–106.
[51] X.F. Tang, J.L. Chen, X.M. Huang, Y.D. Xu, W.J. Shen, Applied Catalysis B: Environmental 81 (2008) 115–121.
[52] G.J. Hutchings, A.A. Mirzaei, R.W. Joyner, M.R.H. Siddiqui, S.H. Taylor, Applied Catalysis A-General 166 (1998) 143–152.
[53] Q.H. Tang, T. Liu, Y.H. Yang, Catalysis Communications 9 (2008) 2570–2573.
[54] A.J. Maira, J.M. Coronado, V. Augugliaro, K.L. Yeung, J.C. Conesa, J. Soria, Journal of Catalysis 202 (2001) 413–420.
[55] S. Ardizzone, C.L. Bianchi, G. Cappelletti, A. Naldoni, C. Pirola, Environmental Science and Technology 42 (2008) 6671–6676.
[56] G. Martra, S. Coluccia, L. Marchese, V. Augugliaro, V. Loddo, L. Palmisano, M. Schiavello, Catalysis Today 53 (1999) 695–702.
[57] Y.B. He, Z.B. Rui, H.B. Ji, Catalysis Communications 14 (2011) 77–81.
[58] F. Konietzni, H.W. Zanthoff, W.F. Maier, Journal of Catalysis 188 (1999) 154–164.